AMERICAN SOCIETY FOR MICROBIOLOGY | Infection and Immunity®

BACTERIAL INFECTIONS

Brucella neotomae Recapitulates Attributes of Zoonotic Human Disease in a Murine Infection Model

Yoon-Suk Kang,[a,b] Daniel A. Brown,[a] James E. Kirby[a,b]

[a]Department of Pathology, Beth Israel Deaconess Medical Center, Boston, Massachusetts, USA
[b]Harvard Medical School, Boston, Massachusetts, USA

ABSTRACT Members of the genus *Brucella* are Gram-negative pathogens that cause chronic systemic infection in farm animals and zoonotic infection in humans. Study of the genus *Brucella* has been hindered by the need for biosafety level 3 select agent containment. *Brucella neotomae*, originally isolated from the desert pack rat, presented an opportunity to develop an alternative, non-select agent experimental model. Our prior *in vitro* work indicated that the cell biology and type IV secretion system (T4SS) dependence of *B. neotomae* intracellular replication were similar to observations for human-pathogenic select agent *Brucella* species. Therefore, here, we investigated the pathobiology of *B. neotomae* infection in the BALB/c mouse. During a sustained infectious course, *B. neotomae* replicated and persisted in reticuloendothelial organs. Bioluminescent imaging and histopathological and PCR-based analysis demonstrated that the T4SS contributed to efficient early infection of the liver, spleen, and lymph nodes; granuloma formation and hepatosplenomegaly; and early induction of Th1-associated cytokine gene expression. The infectious course and pathologies in the murine model showed similarity to prior observations of primate and native host infection with zoonotic *Brucella* species. Therefore, the *B. neotomae* BALB/c infection model offers a promising system to accelerate and complement experimental work in the genus *Brucella*.

KEYWORDS *Brucella*, *Brucella neotomae*, brucellosis, bioluminescent imaging, murine model, pathogenesis, pathology, type IV secretion system, undulant fever

Members of the genus *Brucella*, Gram-negative coccobacilli, cause systemic bacterial infections in domesticated farm animals and other vertebrates (1). Humans may be infected through ingestion of unpasteurized dairy products, inhalation of organisms from birthing farm animals, and during occupational exposure in abattoir and meat packing industries. Disease in humans is characterized by chronicity and a waxing and waning fever (so-called undulant fever). Lymph node infection and enlargement are common (2); endovascular and osteoarticular infection are unwelcome and not infrequent complications (3, 4).

Based on the low aerosol infectious dose and debilitating disease, the major zoonotic species, *Brucella melitensis*, *Brucella abortus*, and *Brucella suis*, are classified as biosafety level 3, category B overlap select agents (5). Biosafety containment and select agent regulations represent significant impediments to experimental investigation.

Brucella organisms have been studied in several *in vitro* and *in vivo* model systems (6–9). *In vitro* assays have demonstrated the capability of *Brucella* species to grow within specialized vacuoles inside of macrophages, endothelial cells, and other cell types. In particular, *Brucella* species alter the normal process of phagosomal maturation. Remodeling of the phagosome occurs in a temporal fashion in which organisms are first found within endocytic vacuoles that subsequently take on properties of the endoplasmic reticulum and autophagosomes and permit intracellular replication (10–14). These events have been found to depend on a bacterial VirB-based type IV secretion

Citation Kang Y-S, Brown DA, Kirby JE. 2019. *Brucella neotomae* recapitulates attributes of zoonotic human disease in a murine infection model. Infect Immun 87:e00255-18. https://doi.org/10.1128/IAI.00255-18.

Editor Craig R. Roy, Yale University School of Medicine

Address correspondence to James E. Kirby, jekirby@bidmc.harvard.edu.

Received 1 April 2018
Returned for modification 27 April 2018
Accepted 23 October 2018
Accepted manuscript posted online 29 October 2018
Published 19 December 2018

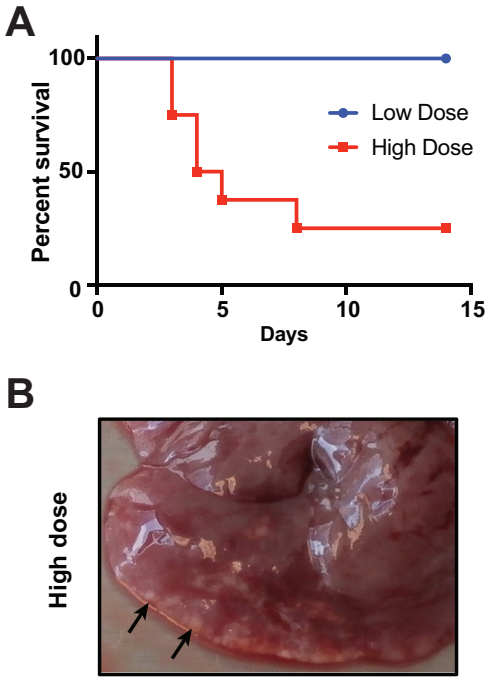

FIG 1 Virulence of *B. neotomae* in BALB/c mice. (A) Two groups of eight mice each were infected i.p. with a low dose (10^6 CFU) or a high dose (10^8 CFU) of *B. neotomae*. Survival was monitored for 2 weeks. (B) Representative image of liver 14 days after high-dose infection in a surviving mouse. The arrows indicate white-tinged granulomas or microabscesses on the liver surface.

system (T4SS) (10–14). Presumably, effectors translocated into the eukaryotic cytoplasm by this secretion apparatus alter phagosome biogenesis to establish an intracellular replication niche. Murine infection by human-pathogenic zoonotic *Brucella* species has also been explored (10, 15–18). In particular, select agents *B. abortus*, *B. melitensis*, and *B. suis* cause sustained T4SS-dependent, high-burden infection in BALB/c mice.

Our specific goal was to establish a non-select agent *Brucella* infection model that would accelerate and complement experimental work in the genus. *Brucella neotomae* was originally isolated from the desert wood rat (19), a pack rat species in the genus *Neotoma*, and has been previously classified as a biosafety level 2 pathogen (13). Importantly, our prior *in vitro* work indicated that the organism replicated efficiently in macrophages in a T4SS-dependent manner and showed temporal phagosome maturation dynamics similar to those of human-pathogenic species (13).

However, the infectious course of *B. neotomae* in laboratory mice remains insufficiently characterized. One prior study found that *B. neotomae* caused sustained infection in BALB/c mice but not in C57BL/6 mice (20), a murine host previously noted to be less hospitable to infection by *Brucella* species (7); however, infectious pathogenesis was not further investigated. Therefore, here, we characterized the microbiology, pathology, and T4SS dependence of *B. neotomae* infection in the BALB/c murine host.

RESULTS

Assessment of virulence of *B. neotomae* in BALB/c mice. The pathogenicity of *B. neotomae* in the BALB/c mouse was initially evaluated during intraperitoneal (i.p.) infection with either 1.0×10^6 or 1.0×10^8 CFU (Fig. 1A). Mice infected with the higher dose showed 75% mortality within 8 days postinfection. In contrast, mice infected at the lower dose all survived ($P = 0.002$ for difference in survival; log-rank Mantel-Cox test). In all the mice surviving high-dose infections, punctate white lesions were observed on the liver surface, consistent with granulomas or microabscesses (Fig. 1B).

Type IV secretion system-dependent *Brucella* virulence. To investigate the role of the T4SS in *B. neotomae* pathogenesis, we infected mice via intraperitoneal injection

with either 10^7 CFU of *B. neotomae* wild type (wt) or Δ*virB4*, a previously described T4SS in-frame deletion mutant that is unable to replicate in cultured J744A.1 macrophages (13). At time intervals spanning 2 months, we monitored CFU in liver, spleen, and thymus. In wt bacterial infection, peak CFU counts were observed at 3 days postinfection in spleen and liver, at levels considerably above the initial inoculum, and 7 days postinfection in thymus, suggesting significant *in vivo* replication during the early infectious period (Fig. 2A to C). CFU decreased thereafter. However, infection was sustained for at least 2 months, with levels of approximately 10^3 CFU at 8 weeks postinfection. During Δ*virB4* bacterial infection, CFU counts at early time points were lower than for wild-type bacterial infection during early infection and were sustained at lower levels at later time points. Notably, Δ*virB4* bacteria were not isolated from the thymus at any time point. These differences reached statistical significance at several time points in liver, spleen, and thymus (as shown in Fig. 2A to C). In contrast, results for the complemented Δ*virB4* strain (virB4c) were not significantly different from wild-type bacterial infection for all comparisons. Taken together, these results suggested that an intact T4SS provided a significant growth advantage during all stages of infection and at all the sites examined. The organism burden was separately quantified by quantitative PCR (qPCR) of the multicopy *B. neotomae* IS*711* insertion sequence for liver and spleen with similar results (Fig. 2D and E). Calculated genome copy numbers were roughly 10-fold higher than CFU counts, suggesting a substantial fraction of unculturable or nonviable organisms.

During infection with the wild-type strain, hepatosplenomegaly was most pronounced at 1 to 2 weeks postinfection (Fig. 2F and G). Liver and splenic organ weights during both wild-type and virB4c infection were statistically greater than uninfected control organ weights at all time points. In contrast, there was no significant difference in liver and spleen weights during infection with the Δ*virB4* mutant in comparison to mock-infected controls of the same age.

To further assess infection dynamics, isogenic wild-type, Δ*virB4*, and complemented Δ*virB4* strains expressing a bacterial luciferase operon (13) were used to infect mice, followed by whole-body bioluminescence imaging (BLI) (Fig. 2H). Wild-type and complemented Δ*virB4* strain signals were maximal at 3 days postinfection and were concentrated in the peritoneal cavity (the inoculation site). On days 3 and 7, there was partial redistribution of bacterial signal to liver, spleen, and lymph nodes. Scattered lymph node positivity was observed at day 14, and no signal was detected at day 28 (data not shown). In contrast, the signal from Δ*virB4* bacterial infection was notably lower than that from infection by the wild type or complemented mutants at the inoculation site from day 1 postinfection onward (Fig. 2E and data not shown). Furthermore, there was no detectable signal in liver, spleen, or lymph nodes at all time points.

Pathologies. Liver and spleen showed significant pathology. Following infection with wild-type *B. neotomae*, there was a prominent granulomatous response in the liver consisting of nodular clusters of histiocytes with occasional lymphocytes and granulocytes (Fig. 3A), with central necrosis observed in granulomas in several mice (Fig. 3B). The spleens demonstrated significant white-pulp expansion (Fig. 3C), most prominent 7 to 14 days postinfection, with one mouse at 14 days postinfection demonstrating a wedge-shaped area of necrosis under the capsule (Fig. 3E), suggestive of an infarct (Fig. 3F). In contrast, in Δ*virB4* bacterial infections, granulomas and splenic white-pulp expansion were not observed (Fig. 3D). As the strains used in the experiments constitutively expressed a tdTomato fluorescent-protein reporter, association of organisms with pathologies could also be assessed by fluorescence microscopy. Specifically, fluorescent organisms were detected within granulomas during wild-type bacterial infection, often in large intracellular clusters suggestive of robust intracellular replication (Fig. 3G). However, during Δ*virB4* bacterial infection, fluorescent organisms were infrequently observed and, when present, were found only individually or in small clusters.

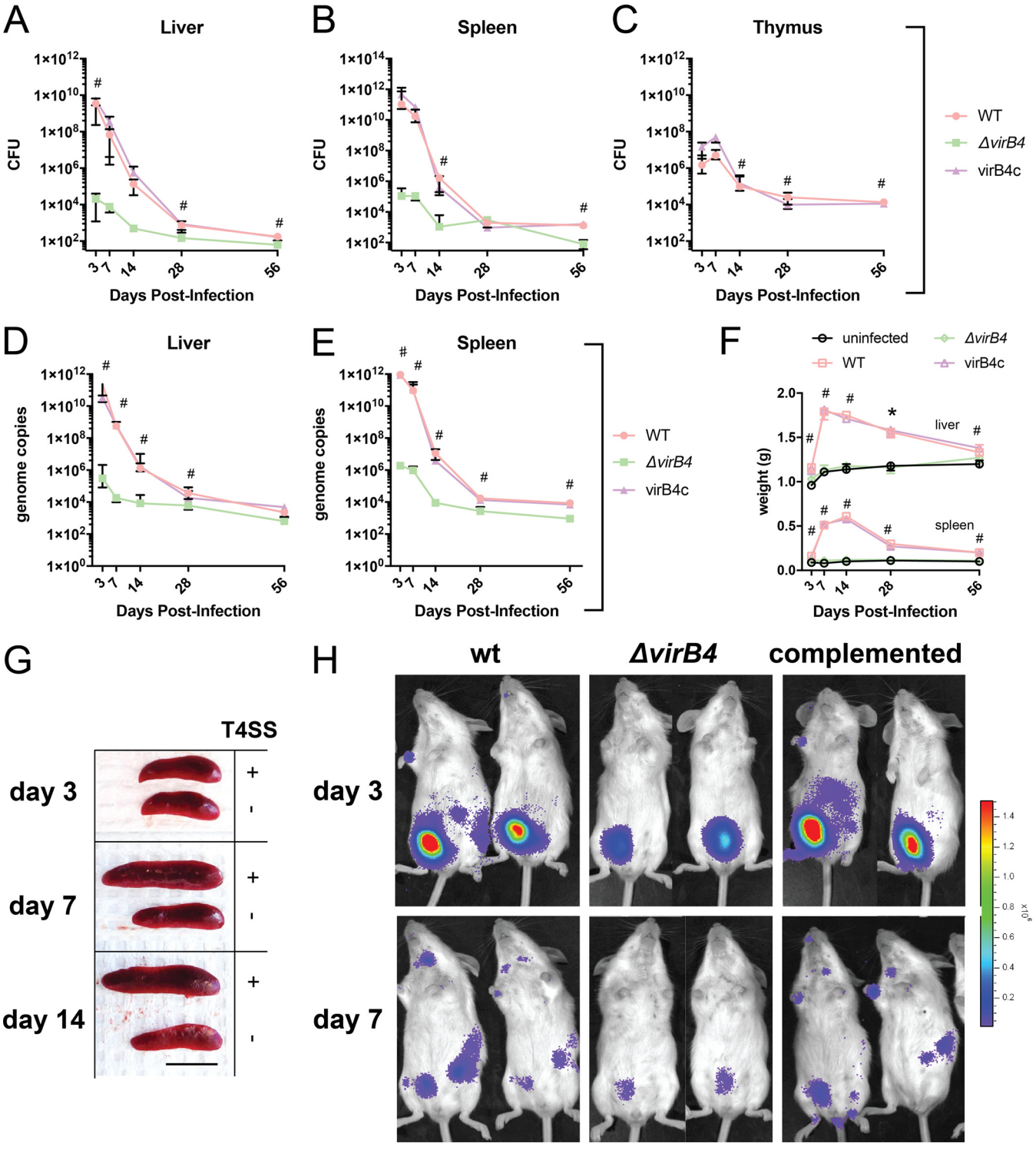

FIG 2 VirB T4SS contributes to pathogenesis. (A to C) Bacterial CFU in liver, spleen, and thymus. (D and E) *B. neotomae* genome copies in liver and spleen. The data shown are the medians and interquartile ranges for five mice per group. #, significant difference between wild-type and Δ*virB4* bacterial infections using Dunn's posttest. There were no statistically significant differences for either CFU or genome copies between wild-type and complemented virB4 (virB4c) infections at any time point. (F) Liver and spleen weights during infection. The data shown are medians and interquartile ranges for five mice per group. #, significant difference between both wild-type and virB4c infections and uninfected controls. Liver and spleen weights were not statistically different between Δ*virB4* strain-infected mice and uninfected control mice at any time point. (G) Representative spleens from infections with wild-type (T4SS$^+$) or Δ*virB4* (T4SS$^-$) strains. Significant splenic enlargement was noted 7 and 14 days following wild-type bacterial infection. Scale bar = 1 cm. (H) Small-animal imaging following infection with bacterial strains with a luciferase operon reporter. The color bar is scaled to a minimum and maximum of 2.0×10^4 and 1.5×10^6 p/s/cm^2/sr, respectively. Two of three mice per infecting strain with maximal signal are shown. Bacterial inocula in all experiments were 10^7 per mouse by intraperitoneal injection.

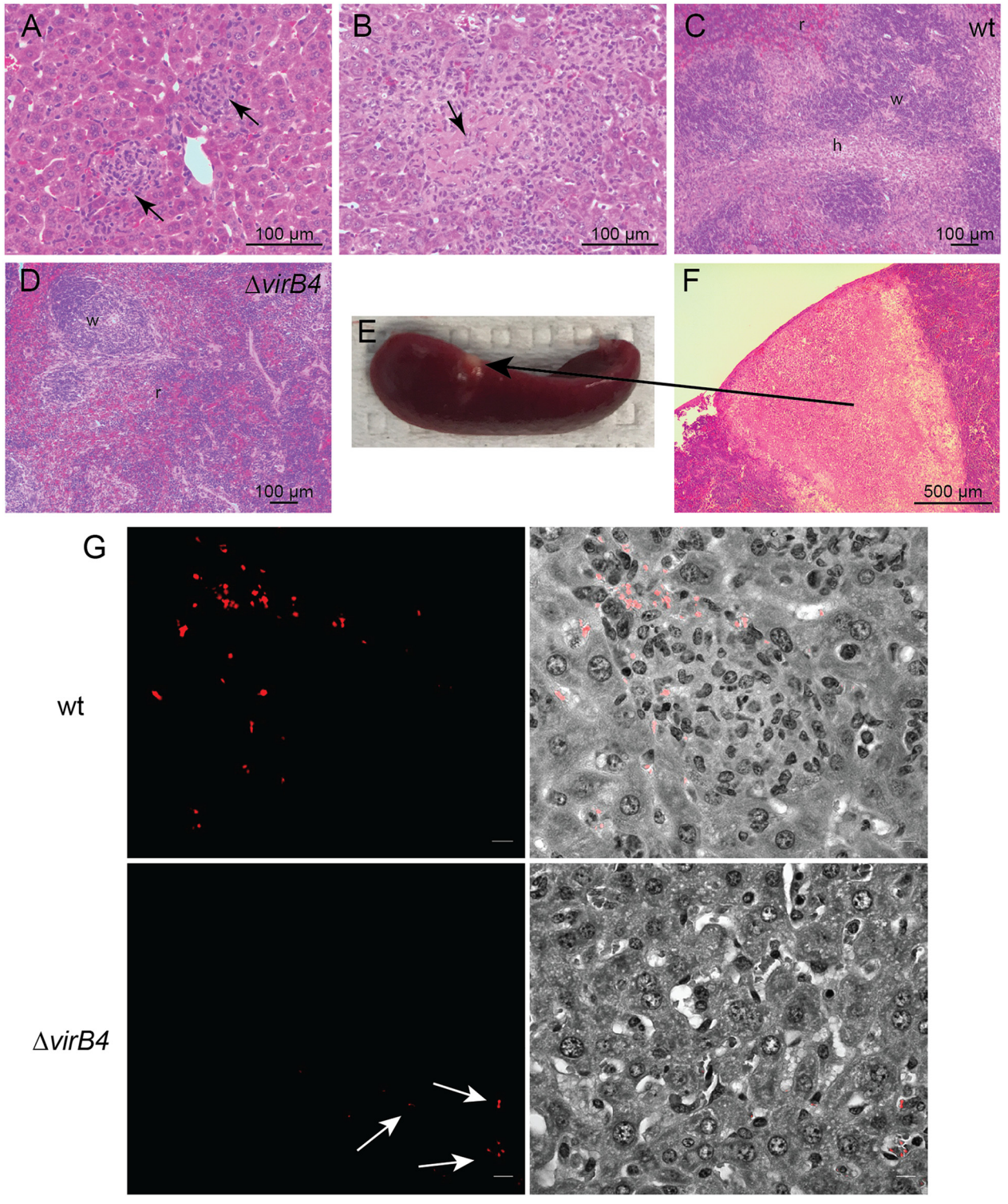

FIG 3 Histopathology of *B. neotomae* infection. (A and B) Granulomatous inflammation (arrows) 3 days (A) and necrotizing granuloma (arrow) 7 days (B) postinfection with wild-type *B. neotomae*. (C) Splenic white-pulp expansion 7 days postinfection with wild-type organisms (w, white pulp; r, red pulp; h, histiocytes). (D) In contrast, white-pulp expansion was not evident following Δ*virB4* bacterial infection. (E and F) Splenic infarct gross pathology (E) and associated microscopic pathology with evidence of tissue necrosis (F) 14 days postinfection with wild-type organisms. (G) (Top) Immunofluorescence microscopy demonstrating intracellular clusters of *B. neotomae* organisms within hepatic granulomas 3 days postinfection with the wild-type strain. (Left) Fluorescent image of bacteria expressing tdTomato fluorescent reporter. (Right) Merged bright-field and gray-scale images. (Bottom) In contrast, only very rare organisms were observed following infection with the Δ*virB4* strain, generally as single organisms or very small clusters (arrows), likely within Kupffer cells lining sinusoidal spaces. Bars = 5 μm.

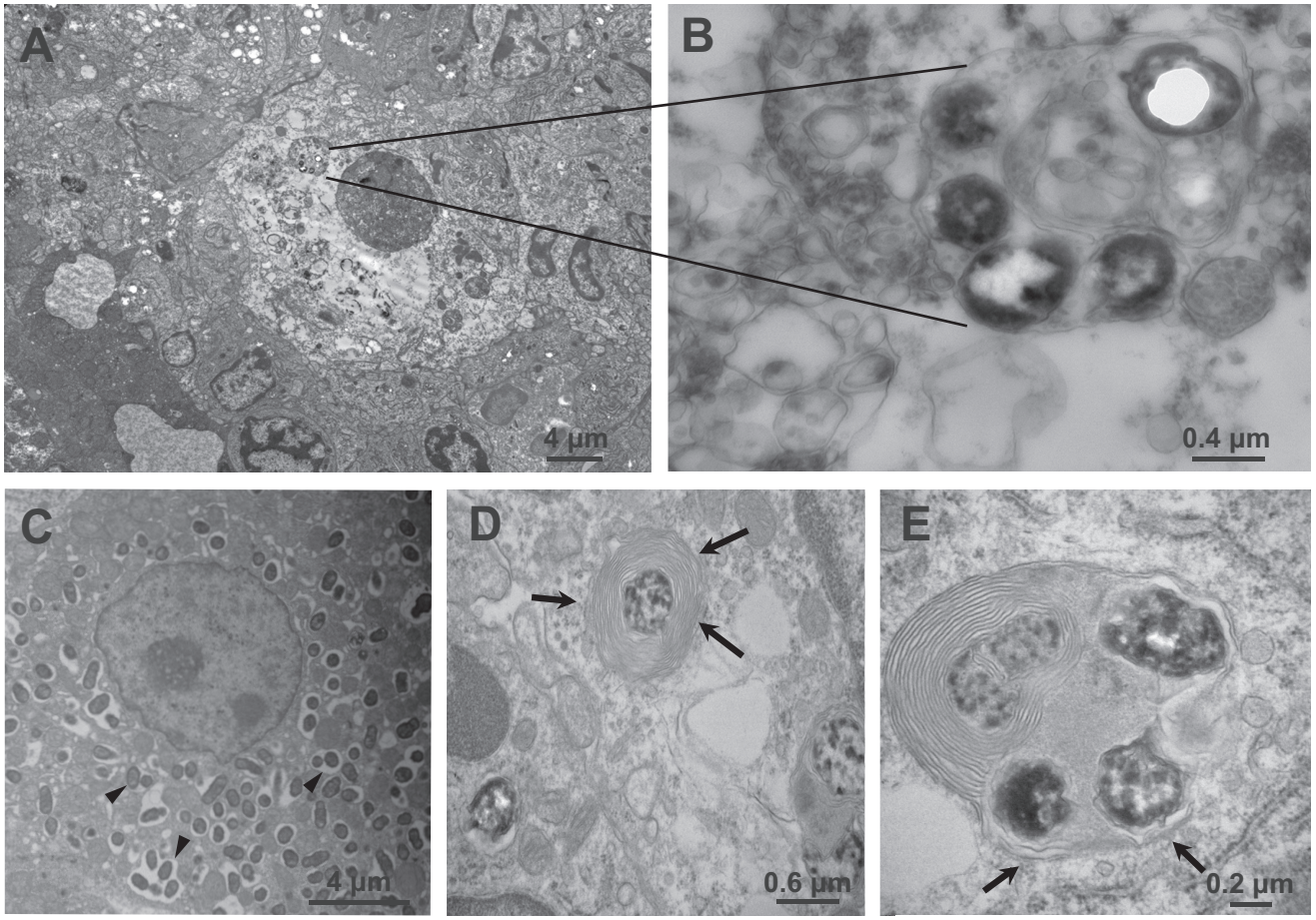

FIG 4 Transmission electron microscopy images of hepatic infection. (A) Hepatic granuloma 3 days postinfection, composed of concentric histiocytes. (B) A central histiocyte appears necrotic and contains a replicative phagosome, inside of which are multiple bacteria. (C to E) *B. neotomae* bacteria replicating inside membrane-bound phagosomes (arrowheads) 7 days postinfection (C) and also found in multilaminar phagosomes (D, arrows) suggestive of autophagosomes or autophagolysosomes in close association with rough endoplasmic reticulum (E, arrows).

Transmission electron microscopy (TEM) was also used to visualize subcellular localization of bacteria in tissues. Bacteria were detected only during infections with the wild-type strain, presumably based on the difficulty in finding a smaller number of Δ*virB4* organisms in ultrathin sections. Figure 4A shows a hepatic granuloma 3 days postinfection consisting of concentric macrophages with a single central necrotic macrophage containing numerous intracellular bacteria in a multilaminar phagosome (Fig. 4B). More generally, phagosomes containing bacteria surrounded by single (Fig. 4C) or multiple (Fig. 4D and E) smooth, concentric layers of membrane were observed, suggestive of autophagosomes (21–23). Rough endoplasmic reticulum was observed in proximity to, but not as a constituent of, phagosomal membranes.

Induction of cytokine gene expression during infection. To determine whether *B. neotomae* infection was associated with a predominant Th1- or Th2-mediated immune response, cytokine gene expression levels in liver and spleen were measured during infection (Fig. 5). Notably, at 3 days postinfection, tumor necrosis factor alpha (TNF-α) and interleukin 2 (IL-2) expression, typically associated with a Th1 response, were significantly upregulated over 10-fold during wt and virB4c infection compared to uninfected controls. Similarly, Toll-like receptor 2 (TLR2), but not TLR4, expression (data not shown) was significantly induced by wt and virB4c at 3 days postinfection but not at later time points. In contrast, Δ*virB4* bacterial infection did not induce significant upregulation of TNF-α, IL-2, or TLR2. At 3 days postinfection, IL-4 expression levels were significantly lower than those of uninfected controls during both wt and Δ*virB4*

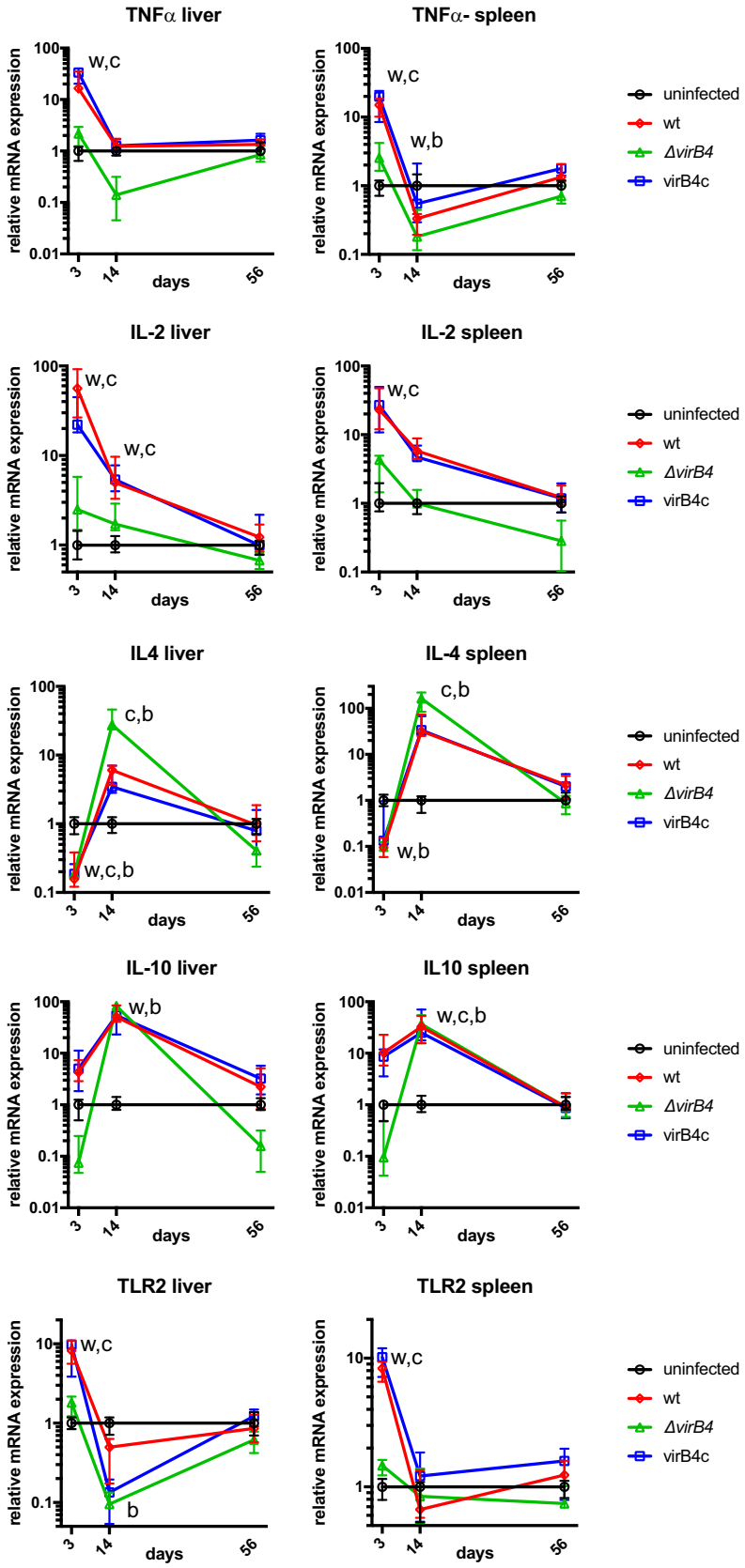

FIG 5 Cytokine gene expression. Cytokine and Toll-like receptor mRNA gene expression was determined in liver and spleen at the indicated times postinfection by reverse transcriptase qPCR. Expression was normalized to actin gene expression within each sample to control for efficiency of mRNA extraction. The

(Continued on next page)

bacterial infections. However, at day 14 postinfection, expression levels induced by wt, virB4c, and Δ*virB4* strains exceeded those of uninfected controls, reaching statistical significance for Δ*virB4* and virB4c infections. A similar statistically significant increase of IL-10 expression was present at day 14 postinfection. Taken together, TNF-α, IL-2, and TLR2 data were consistent with an early T4SS-dependent Th1 response; IL-4 and IL-10 data were consistent with a delayed, T4SS-independent Th2 response.

DISCUSSION

Here, we describe microbiological and pathological features of murine *B. neotomae* infection. Several aspects of T4SS-driven pathogenesis were evident by complementary analyses, including persistent infection of the reticuloendothelial organs, intracellular replication within granulomas, and early induction of a Th1 cytokine transcriptional response.

It is worthwhile discussing results in the context of prior observations for the species and genus. Five independent strains of *B. neotomae* were originally isolated from tissues of 108 desert wood rats from Utah (19), including the type strain, 5K33, used in our studies. Five additional isolates from desert wood rats and a sixth from a desert wood rat flea were also described separately by Thorpe et al. (24). These observations indicate a substantial prevalence (~5%) of *B. neotomae* in U.S. desert pack rats (genus *Neotomae*). Transmission among animals was not observed under laboratory conditions, and therefore, the natural modes of transmission are far from clear (24).

In prior experimental work, *B. neotomae* was noted to cause sustained infection in *Mus musculus*, *Neotoma lepida* (desert wood rat), and guinea pigs for periods as long as 18 to 24 months (24). The minimal infectious dose during intraperitoneal inoculation of mice was noted to be only several organisms (19). In contrast, in limited experiments, rabbits, cows, sheep, swine, and mule deer were noted to be relatively resistant to infection (24, 25). Low-inoculum infectivity and sustained infection by *B. neotomae*, therefore, occurred most readily in rodents.

Although not previously thought capable of infecting humans, *B. neotomae* was recently isolated from the cerebrospinal fluid of two patients from Costa Rica (26). Potential epidemiological associations and patient comorbidities were not investigated. Therefore, the mechanism of infection and risk factors are uncertain. It is notable that human contact with pack rat middens (nests) is presumably not insignificant, yet there have been only two documented infections, and none in the area of known endemicity, potentially consistent with lower pathogenic potential in humans. Nevertheless, *B. neotomae* now assumes importance as a rare, and likely underrecognized, zoonotic pathogen capable of causing serious disease in humans.

In our experiments, the *B. neotomae* infectious course in BALB/c mice showed similarity to *B. abortus*, *B. melitensis*, and *B. suis* infection of domesticated farm animals and primates. For example, during aerosol infection of rhesus monkeys with *B. melitensis* with inocula ranging generally from 10^5 to 6×10^6 organisms, both liver and spleen CFU were prominent early in infection (27–29); liver counts dropped from 10^6 to 10^4 CFU from days 15 to 45 (29); and organisms were isolated at low levels from liver and spleen 8 to 9 weeks after infection (27, 28), similar to observations in the *B. neotomae* murine model. Additionally, significant quantities of organisms were isolated from lymph nodes during *B. melitensis* infection of rhesus monkeys; during *B. abortus* strain 1308 and/or 544 McEwen infection of cows and bison (30–32); and during human infection, especially in children (33, 34). Therefore, the infectious course of *B. neotomae* in BALB/c mice and, in particular, the sustained low organism burden and lymph node

FIG 5 Legend (Continued)
data points are plotted relative to the median gene expression from uninfected mice and represent the medians and interquartile ranges of values from five mice per group. w, significant difference between wild-type bacterial infection and a mock-infected control; c, significant difference between virB4c infection and an uninfected control; b, significant difference between Δ*virB4* bacterial infection and an uninfected control.

colonization observed by bioluminescent imaging, appear similar to other examples of native host infection. These findings may reflect the relative relatedness of *M. musculus* to the native desert pack rat host.

It has been observed previously that *Brucella* species highly pathogenic for humans display a distinct infectious course in BALB/c mice. Specifically, high-level splenic infection of at least 10^6 CFU per organ peaks at 2 to 3 weeks postinfection and is sustained for months (7, 35). In contrast, organisms are cleared from the liver within 1 month (7). As mentioned previously, these findings differ from the chronic lower burden of infection observed in native hosts (and humans infected with *B. abortus*, *B. melitensis*, and *B. suis* [1]) and from *B. neotomae* in the BALB/c model. Findings for *B. neotomae*, however, were similar to observations of BALB/c infection with the attenuated *B. abortus* S19 vaccine strain and *Brucella ceti* (7, 36, 37), a cetacean pathogen. S19 (7) and *B. neotomae* murine infection (this study) also are both associated with maximum splenic enlargement at 2 weeks. This contrasted with virulent *B. abortus* 2308 murine infection, in which spleen weight gradually increases during the course of prolonged infection (7). Therefore, the absence of sustained splenic infection and splenomegaly during murine *B. neotomae* infection was consistent with a pattern associated with *Brucella* strains and species with lower infectivity and pathogenic potential for humans (7).

The T4SS plays an important role during murine infection with *Brucella* species (10–14, 38–40). Interestingly, *B. neotomae* Δ*virB4* infection showed both quantitative and qualitative attenuation, the latter, as observed during BLI studies, suggesting that T4SS contributes to colonization of the reticuloendothelial system (lymph nodes, spleen, and liver). We did not sample lymph nodes for CFU analysis; however, the absence of Δ*virB4* CFU isolated from the thymus, a site of long-term *Brucella* colonization in animals where examined (34, 41, 42), at any time point also supports a dissemination defect. This qualitative phenotype is reminiscent of the previously observed VirB-dependent colonization of mesenteric lymph nodes, spleen, and liver after gastrointestinal infection of BALB/c mice with *B. melitensis* 16 M (39) and the VirB-dependent reticuloendothelial system colonization of C57BL/6 mice by *B. melitensis* after intraperitoneal infection (40).

B. neotomae infection was associated with a granulomatous immune response most evident in the liver, also observed during human infection (43, 44) and infection of mice with zoonotic and attenuated *Brucella* species and strains (7). Related to these observations, the pattern of inflammatory cytokine transcriptional induction by *B. neotomae* during early infection was consistent with a *virB4*-dependent Th1 response previously observed during murine infection (45–47), a Th1 response observed during human infection (48), and the known association of Th1 cytokine induction with a granulomatous response to chronic bacterial infections (49). Expression of TLR2, but not TLR4, was also markedly induced during early infection with $T4SS^+$ organisms. This finding was notable, given the previously described TLR2 dependence of the Th1 cytokine response to *B. abortus* in mice (50). The selective induction of TLR2 may potentially be explained by the previously described induction of TLR2, but not TLR4, gene expression in murine macrophages by inflammatory cytokines and lipopolysaccharide (51).

There were several limitations to our studies. For BLI, bacteria were labeled with a constitutively expressed bacterial luciferase operon. Luminescence depends on substrate production and the cellular ATP level. Therefore, discrepancies between BLI and CFU counts may be partially accounted for by the culturability and metabolism of organisms, which may differ by body site. Furthermore, BLI intrinsically has much lower sensitivity than both CFU counts and qPCR and therefore cannot provide information on low-burden chronic infection. In addition, the peritoneal cavity and lymph nodes, areas of BLI intensity, were not systematically sampled for CFU counts and histopathological analysis, a goal for future work with this model. Furthermore, bacteria were observed only rarely by TEM, and therefore, ultrastructural observations of phagosomal properties may have been subject to sampling bias. Relatively high inocula were used for infections, and it is possible that the disease course and pathologies would have

been different with lower inocula. Cytokine gene expression was measured in whole organs. Systemic cytokine loads and expression in individual cell types were not measured and might have provided a different and more nuanced readout. Nevertheless, our results are consistent with the Th1-type predominant early cytokine response observed in other models. Finally, only one of the original *B. neotomae* strains isolated by Stoenner and Lackman (19) and Thorpe et al. (24) remains available: strain 5K33, used in our studies. Therefore, extension of our findings to other *B. neotomae* isolates would be of interest as future strains become available.

In summary, we found that the *B. neotomae* murine model recapitulates attributes of infection caused by *Brucella* species that are highly pathogenic for humans and native hosts. Importantly, *B. neotomae* is neither a biosafety level 3 pathogen nor a select agent. Therefore, we believe it can be safely handled with enhanced biosafety level 2 practices (13), thereby greatly simplifying logistics and accelerating scientific investigation. As such, the *B. neotomae* murine infection model should provide an informative and tractable *in vivo* model system for investigation of *Brucella* pathogenesis.

MATERIALS AND METHODS

Bacterial strains and growth conditions. *B. neotomae* 5K33 (BEI Resources, Manassas, VA) and isogenic Δ*virB4* mutant strains constitutively expressing a chromosomally integrated tdTomato fluorescent protein reporter or a *lux* operon reporter, both linked to a nourseothricin resistance cassette, were described previously (13). A complemented Δ*virB4* mutant (virB4c) with the *virB4* gene expressed constitutively from the broad-host-range, stable pBMTL2 plasmid, was also previously described and characterized *in vitro* (13). Prior to the experiments, *Brucella* strains, stored at −80°C, were passaged on sheep blood agar and grown overnight in tryptic soy broth (BD Biosciences, Franklin Lakes, NJ) at 37°C with 5% CO_2 in a shaking incubator.

Murine infection. Mouse experiments were performed under an institutional animal care and use committee-approved protocol. BALB/c mice (Charles River Laboratories, Wilmington, MA), 4 to 6 weeks of age, were infected through i.p. inoculation. To prepare infectious inocula, 1 ml of overnight *Brucella* culture was pelleted, washed twice with phosphate-buffered saline (PBS), and adjusted to the desired inoculum in 100 μl PBS based on an empirically determined correspondence of an optical density at 600 nm (OD_{600}) of 1.0 to approximately 3×10^9 CFU/ml. At the indicated time points, mouse organs were harvested and homogenized in 1 ml of PBS (pH 7.2) using a sterile 15-ml conical tissue grinder (Biomedical Polymers, Gardner, MA). Serial dilutions of the homogenates were plated on tryptic soy agar (TSA) containing 50 μg/ml nourseothricin for CFU determination.

Whole-mouse imaging. Whole-mouse imaging was performed on a Xenogen IVIS-50TM imaging system with Living Image software using a 3-min exposure and a field of view of 12 cm. The system software quantifies the total luminescence flux signal (photons [p] per second) and displays average radiance intensity (photons per second per square centimeter per steradian [sr]) using a color-coded histogram with user-defined minimum and maximum signal thresholds.

qPCR analysis. For qPCR experiments to quantify *B. neotomae* in tissues, 50 mg of each tissue sample was extracted using a DNeasy Blood and Tissue kit (Qiagen, Valencia, CA) according to the manufacturer's instructions. Primers GCCTCCAGTCGATTGTTGGGGCAC and GTGACTGTCCGCAAGCTTCAAGCC amplify a 177-bp fragment within IS*711* and were identified based on multiple-sequence alignment of IS*711* elements from *Brucella* sp. strain B14/94, *B. ceti* B1/94, *B. pinnipedialis* B2/94, *B. abortus* B12, and *B. abortus* B16 (GenBank accession numbers AF242534, FJ376557, FJ376556, JF345125, and JF345126, respectively) using the Lasergene software package (DNAStar, Madison, WI). The reagents in the DyNAmo HS SYBR Green qPCR kit (Thermo Scientific) were used to set up qPCRs. Cycling and detection were performed on a CFX 384 real-time PCR detection system (Bio-Rad, Hercules, CA) with an initial 95°C denaturation for 5 min, followed by 40 cycles of 95°C for 15 s and 60°C for 40 s.

To convert quantification cycle (C_q) values obtained during real-time PCR detection to *B. neotomae* genome equivalents, a 354-bp fragment of IS*711* from *B. neotomae* was amplified using primers CGCG AATTCGAGACCCATGAATGCGGTCAA and CGCGTCGACACGACCAAGCTGCATGCTGTT and cloned into the EcoRI/SalI restriction sites of the pMOD3 vector (Epicentre, Madison, WI). Plasmid DNA was extracted using a QIAprep miniprep kit (Qiagen, Valencia, CA), quantified using a NanoDrop 1000 spectrophotometer (Thermo Scientific, Waltham, MA), serially diluted, and analyzed by qPCR to establish a correspondence between C_q values and IS*711* quantity. Following qPCR of tissue samples, the IS*711* quantity was then determined based on the calibration curve and converted to *B. neotomae* genome equivalents by dividing by the IS*711* copy number in *B. neotomae* 5K33 ($n = 8$) inferred from previously published Southern blots (52) and the genome sequence (accession number KN046827.1).

Frozen-section fluorescence microscopy. Tissue immersed in OCT compound (Sakura Finetek USA, Inc., Torrance, CA) was frozen in liquid nitrogen on a Tissue-Tek cryomold (Sakura Finetek). Frozen sections (10 μm thick) were then cut using a Leica CM3050s cryostat (Leica Biosystems, Buffalo Grove, IL), applied to Superfrost Plus glass slides (Fisher Scientific, Hampton, NH), and fixed with 4% formaldehyde at 4°C for 12 h. The fixed sections were washed twice with PBS, stained in Gill's hematoxylin solution no. 3 (Fisher Scientific) for 3 min, washed in tap water for 5 min, immersed in Scott's bluing solution for 3

min (53, 54), and counterstained with alcoholic Eosin Y (Fisher Scientific) for 3 min. Tissue sections were subsequently dehydrated with graded series of ethanol, cleared with xylene, and coverslipped.

Visualization of tdTomato-expressing bacteria was performed using a Zeiss LSM 880 confocal microscope (Carl Zeiss Microscopy, Thornwood, NY) with a 562.5- to 587.5-nm bandpass filter as previously described (13). The microscope PMT (photomultiplier tube) setting was used to detect corresponding bright-field images.

Electron microscopy. Organ specimens were fixed in Trump's fixative containing 4% formaldehyde and 1% glutaraldehyde, washed in 0.1 M cacodylate buffer, and postfixed in 1% OsO_4 as described previously (55). Samples were then dehydrated in ascending alcohol washes and embedded in Eponate 12 resin (Ted Pella, Inc., Redding, CA). Digital images of ultrathin sections were acquired with a Jeol (Tokyo, Japan) MEM-1011 transmission electron microscope.

Cytokine mRNA expression. Total RNA was extracted from liver and spleen tissue using an RNeasy Mini kit (Qiagen) according to the manufacturer's instructions. After RNA elution, reverse transcription-quantitative PCR (RT-qPCR) was performed to determine relative transcription of cytokine-related murine genes normalized to β-actin expression. The following primer sets designed with the Integrated DNA Technologies (Skokie, IL) PrimerQuest tool were used (forward primer, reverse primer, and murine gene accession number): IL-2 (TGAGCAGGATGGAGAATTACAG, GAGGTCCAAGTTCATCTTCTAGG, NM_008366), IL-4 (TTGAGAGAGATCATCGGCATTT, CTCACTCTCTGTGGTGTTCTTC, NM_021283), IL-10 (AACATACTGCTA ACCGACTCC, TCCTTGATTTCTGGGCCATG, NM_010548.2), TNF-α (GTTGTACCTTGTCTACTCCCAG, GGTTGA CTTTCTCCTGGTATGAG, NM_013693.3), TLR2 (CACTATCCGGAGGTTGCATATC, GGAAGACCTTGCTGTTCTC TAC, NM_011905), TLR4 (CAGCAGAGGAGAAAGCATCTAT, GTAGTGAAGGCAGAGGTGAAA, NM_021297), and β-actin (GTGGGAATGGGTCAGAAGG, AGCTCATTGTAGAAGGTGTGG, NM_007393.5). Briefly, cDNA synthesis was performed using 2 μg of total RNA, a random primer mixture, and Moloney murine leukemia virus (MMuLV) reverse transcriptase (New England Biolabs). Subsequent qPCR was performed with the DyNAmo HS SYBR Green qPCR kit, 1 μl of cDNA, and 0.2 μM primers. Cycling condition were 3 min at 95°C, followed by 35 cycles of 45 s at 95°C, 45 s at 55°C, and 45 s at 72°C, followed by 10 min at 72°C.

Statistics. Unless otherwise specified, the nonparametric Kruskal-Wallis analysis of variance (ANOVA) test was performed, followed by Dunn's test for *post hoc* comparisons with control groups, using Prism 7 for Mac OSX (GraphPad Software, Inc., La Jolla, CA). A P value of $\leq$0.050 was considered statistically significant.

ACKNOWLEDGMENTS

We acknowledge Meaghan Fox and John-Mac Mroczka from the Beth Israel Deaconess Medical Small Animal Imaging Facility for their expertise. We also thank Katelyn Zulauf and Kenneth Smith for thoughtful comments on the manuscript.

This work was supported by the National Institute of Allergy and Infectious Diseases of the National Institutes of Health under award number R01 AI099122 to J.E.K.

The content is solely our responsibility and does not necessarily represent the official views of the National Institutes of Health.

REFERENCES

1. Dalrymple-Champneys W. 1960. Brucella infection and undulant fever in man. Oxford University Press, London, United Kingdom.
2. Varona JF, Guerra JM, Guillen V, Guillen S, Menassa A, Palenque E. 2002. Isolated cervical lymphadenopathy as unique manifestation of brucellosis. Scand J Infect Dis 34:538–540. https://doi.org/10.1080/00365540232020880 2.
3. Jeroudi MO, Halim MA, Harder EJ, Al-Siba'i MB, Ziady G, Mercer EN. 1987. *Brucella* endocarditis. Br Heart J 58:279–283. https://doi.org/10.1136/hrt.58.3.279.
4. Rajapakse CN. 1995. Bacterial infections: osteoarticular brucellosis. Baillieres Clin Rheumatol 9:161–177. https://doi.org/10.1016/S0950-3579(05)80153-0.
5. Gutierrez MG, Master SS, Singh SB, Taylor GA, Colombo MI, Deretic V. 2004. Autophagy is a defense mechanism inhibiting BCG and *Mycobacterium tuberculosis* survival in infected macrophages. Cell 119:753–766. https://doi.org/10.1016/j.cell.2004.11.038.
6. Celli J, de Chastellier C, Franchini DM, Pizarro-Cerda J, Moreno E, Gorvel JP. 2003. *Brucella* evades macrophage killing via VirB-dependent sustained interactions with the endoplasmic reticulum. J Exp Med 198:545–556. https://doi.org/10.1084/jem.20030088.
7. Grillo MJ, Blasco JM, Gorvel JP, Moriyon I, Moreno E. 2012. What have we learned from brucellosis in the mouse model? Vet Res 43:29. https://doi.org/10.1186/1297-9716-43-29.
8. Myeni S, Child R, Ng TW, Kupko JJ III, Wehrly TD, Porcella SF, Knodler LA, Celli J. 2013. *Brucella* modulates secretory trafficking via multiple type IV secretion effector proteins. PLoS Pathog 9:e1003556. https://doi.org/10.1371/journal.ppat.1003556.
9. Starr T, Child R, Wehrly TD, Hansen B, Hwang S, López-Otin C, Virgin HW, Celli J. 2012. Selective subversion of autophagy complexes facilitates completion of the brucella intracellular cycle. Cell Host Microbe 11:33–45. https://doi.org/10.1016/j.chom.2011.12.002.
10. Hanna N, Jiménez de Bagüés MP, Ouahrani-Bettache S, El Yakhlifi Z, Köhler S, Occhialini A. 2011. The virB operon is essential for lethality of *Brucella microti* in the Balb/c murine model of infection. J Infect Dis 203:1129–1135. https://doi.org/10.1093/infdis/jiq163.
11. Sun YH, den Hartigh AB, Santos RL, Adams LG, Tsolis RM. 2002. *virB*-Mediated survival of *Brucella abortus* in mice and macrophages is independent of a functional inducible nitric oxide synthase or NADPH oxidase in macrophages. Infect Immun 70:4826–4832. https://doi.org/10.1128/IAI.70.9.4826-4832.2002.
12. Rolán HG, Tsolis RM. 2007. Mice lacking components of adaptive immunity show increased *Brucella abortus virB* mutant colonization. Infect Immun 75:2965–2973. https://doi.org/10.1128/IAI.01896-06.
13. Kang YS, Kirby JE. 2017. Promotion and rescue of intracellular *Brucella neotomae* replication during coinfection with *Legionella pneumophila*. Infect Immun 85:e00991-16. https://doi.org/10.1128/IAI.00991-16.
14. Palomares-Resendiz E, Arellano-Reynoso B, Hernandez-Castro R, Tenorio-Gutierrez V, Salas-Tellez E, Suarez-Guemes F, Diaz-Aparicio E. 2012. Immunogenic response of *Brucella canis* virB10 and virB11 mutants in a murine model. Front Cell Infect Microbiol 2:35.

15. Montaraz JA, Winter AJ. 1986. Comparison of living and nonliving vaccines for *Brucella abortus* in BALB/c mice. Infect Immun 53:245–251.
16. Edmonds MD, Cloeckaert A, Elzer PH. 2002. *Brucella* species lacking the major outer membrane protein Omp25 are attenuated in mice and protect against *Brucella melitensis* and *Brucella ovis*. Vet Microbiol 88: 205–221. https://doi.org/10.1016/S0378-1135(02)00110-4.
17. Jimenez de Bagues MP, Iturralde M, Arias MA, Pardo J, Cloeckaert A, Zygmunt MS. 2014. The new strains *Brucella inopinata* BO1 and *Brucella* species 83-210 behave biologically like classic infectious *Brucella* species and cause death in murine models of infection. J Infect Dis 210:467–472. https://doi.org/10.1093/infdis/jiu102.
18. Jiménez de Bagüés MP, Ouahrani-Bettache S, Quintana JF, Mitjana O, Hanna N, Bessoles S, Sanchez F, Scholz HC, Lafont V, Köhler S, Occhialini A. 2010. The new species *Brucella microti* replicates in macrophages and causes death in murine models of infection. J Infect Dis 202:3–10. https://doi.org/10.1086/653084.
19. Stoenner HG, Lackman DB. 1957. A new species of brucella isolated from the desert wood rat, *Neotoma lepida Thomas*. Am J Vet Res 18:947–951.
20. Moustafa DA, Jain N, Sriranganathan N, Vemulapalli R. 2010. Identification of a single-nucleotide insertion in the promoter region affecting the *sodC* promoter activity in *Brucella neotomae*. PLoS One 5:e14112. https://doi.org/10.1371/journal.pone.0014112.
21. Dunn WA. 1994. Autophagy and related mechanisms of lysosome-mediated protein degradation. Trends Cell Biol 4:139–143. https://doi.org/10.1016/0962-8924(94)90069-8.
22. Shin DM, Jeon BY, Lee HM, Jin HS, Yuk JM, Song CH, Lee SH, Lee ZW, Cho SN, Kim JM, Friedman RL, Jo EK. 2010. *Mycobacterium tuberculosis eis* regulates autophagy, inflammation, and cell death through redox-dependent signaling. PLoS Pathog 6:e1001230. https://doi.org/10.1371/journal.ppat.1001230.
23. Detilleux PG, Deyoe BL, Cheville NF. 1990. Entry and intracellular localization of *Brucella* spp. in Vero cells: fluorescence and electron microscopy. Vet Pathol 27:317–328. https://doi.org/10.1177/030098589002700503.
24. Thorpe BD, Sidwell RW, Lundgren DL. 1967. Experimental studies with four species of *Brucella* in selected wildlife, laboratory, and domestic animals. Am J Trop Med Hyg 16:665–674. https://doi.org/10.4269/ajtmh.1967.16.665.
25. Beal GA, Lewis RE, McCullough NB, Claflin RM. 1959. Experimental infection of swine with *Brucella neotomae*. Am J Vet Res 20:872–875.
26. Suárez-Esquivel M, Ruiz-Villalobos N, Jiménez-Rojas C, Barquero-Calvo E, Chacón-Díaz C, Víquez-Ruiz E, Rojas-Campos N, Baker KS, Oviedo-Sánchez G, Amuy E, Chaves-Olarte E, Thomson NR, Moreno E, Guzmán-Verri C. 2017. *Brucella neotomae* infection in humans, Costa Rica. Emerg Infect Dis 23:997–1000. https://doi.org/10.3201/eid2306.162018.
27. Mense MG, Borschel RH, Wilhelmsen CL, Pitt ML, Hoover DL. 2004. Pathologic changes associated with brucellosis experimentally induced by aerosol exposure in rhesus macaques (*Macaca mulatta*). Am J Vet Res 65:644–652. https://doi.org/10.2460/ajvr.2004.65.644.
28. Henning LN, Miller SM, Pak DH, Lindsay A, Fisher DA, Barnewall RE, Briscoe CM, Anderson MS, Warren RL. 2012. Pathophysiology of the rhesus macaque model for inhalational brucellosis. Infect Immun 80: 298–310. https://doi.org/10.1128/IAI.05878-11.
29. Russell-Lodrigue KE, Killeen SZ, Ficht TA, Roy CJ. 2018. Mucosal bacterial dissemination in a rhesus macaque model of experimental brucellosis. J Med Primatol 47:75–77. https://doi.org/10.1111/jmp.12282.
30. Xavier MN, Paixão TA, Poester FP, Lage AP, Santos RL. 2009. Pathological, immunohistochemical and bacteriological study of tissues and milk of cows and fetuses experimentally infected with *Brucella abortus*. J Comp Pathol 140:149–157. https://doi.org/10.1016/j.jcpa.2008.10.004.
31. Davis DS, Templeton JW, Ficht TA, Williams JD, Kopec JD, Adams LG. 1990. *Brucella abortus* in captive bison. I. Serology, bacteriology, pathogenesis, and transmission to cattle. J Wildl Dis 26:360–371. https://doi.org/10.7589/0090-3558-26.3.360.
32. Payne JM. 1959. The pathogenesis of experimental brucellosis in the pregnant cow. J Pathol Bacteriol 78:447–463. https://doi.org/10.1002/path.1700780211.
33. Poston MA, Parsons PB. 1940. Isolation of *Brucella* from lymph nodes. J Infect Dis 66:86–90. https://doi.org/10.1093/infdis/66.1.86.
34. von Bargen K, Gagnaire A, Arce-Gorvel V, de Bovis B, Baudimont F, Chasson L, Bosilkovski M, Papadopoulos A, Martirosyan A, Henri S, Mège JL, Malissen B, Gorvel JP. 2015. Cervical lymph nodes as a selective niche for Brucella during oral infections. PLoS One 10:e0121790. https://doi.org/10.1371/journal.pone.0121790.
35. Crawford RM, Van De Verg L, Yuan L, Hadfield TL, Warren RL, Drazek ES, Houng HH, Hammack C, Sasala K, Polsinelli T, Thompson J, Hoover DL. 1996. Deletion of *purE* attenuates *Brucella melitensis* infection in mice. Infect Immun 64:2188–2192.
36. Mackaness GB. 1964. The immunological basis of acquired cellular resistance. J Exp Med 120:105–120. https://doi.org/10.1084/jem.120.1.105.
37. Nymo IH, Arias MA, Pardo J, Álvarez MP, Alcaraz A, Godfroid J, Jiménez de Bagüés MP. 2016. Marine mammal *Brucella* reference strains are attenuated in a BALB/c mouse model. PLoS One 11:e0150432. https://doi.org/10.1371/journal.pone.0150432.
38. den Hartigh AB, Rolán HG, de Jong MF, Tsolis RM. 2008. VirB3 to VirB6 and VirB8 to VirB11, but not VirB7, are essential for mediating persistence of *Brucella* in the reticuloendothelial system. J Bacteriol 190: 4427–4436. https://doi.org/10.1128/JB.00406-08.
39. Paixão TA, Roux CM, den Hartigh AB, Sankaran-Walters S, Dandekar S, Santos RL, Tsolis RM. 2009. Establishment of systemic *Brucella melitensis* infection through the digestive tract requires urease, the type IV secretion system, and lipopolysaccharide O antigen. Infect Immun 77: 4197–4208. https://doi.org/10.1128/IAI.00417-09.
40. Rajashekara G, Glover DA, Krepps M, Splitter GA. 2005. Temporal analysis of pathogenic events in virulent and avirulent *Brucella melitensis* infections. Cell Microbiol 7:1459–1473. https://doi.org/10.1111/j.1462-5822.2005.00570.x.
41. Tessaro SV, Forbes LB. 2004. Experimental *Brucella abortus* infection in wolves. J Wildl Dis 40:60–65. https://doi.org/10.7589/0090-3558-40.1.60.
42. Ozkaraca M, Ceribasi S, Ceribasi AO, Kilic A, Ongor H. 2016. The role of apoptosis and autophagy in bovine abortions associated with *Brucella* spp. Acta Veterinaria 66:37–50. https://doi.org/10.1515/acve-2016-0003.
43. Hunt AC, Bothwell PW. 1967. Histological findings in human brucellosis. J Clin Pathol 20:267–272. https://doi.org/10.1136/jcp.20.3.267.
44. Cohen FB, Robins B, Lipstein W. 1957. Isolation of *Brucella abortus* by percutaneous liver biopsy. N Engl J Med 257:228–230. https://doi.org/10.1056/NEJM195708012570508.
45. Im YB, Park WB, Jung M, Kim S, Yoo HS. 2016. Evaluation of Th1/Th2-related immune response against recombinant proteins of *Brucella abortus* infection in mice. J Microbiol Biotechnol 26:1132–1139. https://doi.org/10.4014/jmb.1512.12046.
46. Agranovich I, Scott DE, Terle D, Lee K, Golding B. 1999. Down-regulation of Th2 responses by *Brucella abortus*, a strong Th1 stimulus, correlates with alterations in the B7.2-CD28 pathway. Infect Immun 67:4418–4426.
47. Rolan HG, Tsolis RM. 2008. Inactivation of the type IV secretion system reduces the Th1 polarization of the immune response to *Brucella abortus* infection. Infect Immun 76:3207–3213. https://doi.org/10.1128/IAI.00203-08.
48. Rodríguez-Zapata M, Matías MJ, Prieto A, Jonde MA, Monserrat J, Sánchez L, Reyes E, De la Hera A, Alvarez-Mon M. 2010. Human brucellosis is characterized by an intense Th1 profile associated with a defective monocyte function. Infect Immun 78:3272–3279. https://doi.org/10.1128/IAI.01385-09.
49. Roach DR, Bean AG, Demangel C, France MP, Briscoe H, Britton WJ. 2002. TNF regulates chemokine induction essential for cell recruitment, granuloma formation, and clearance of mycobacterial infection. J Immunol 168:4620–4627. https://doi.org/10.4049/jimmunol.168.9.4620.
50. Ferrero MC, Hielpos MS, Carvalho NB, Barrionuevo P, Corsetti PP, Giambartolomei GH, Oliveira SC, Baldi PC. 2014. Key role of Toll-like receptor 2 in the inflammatory response and major histocompatibility complex class II downregulation in *Brucella abortus*-infected alveolar macrophages. Infect Immun 82:626–639. https://doi.org/10.1128/IAI.01237-13.
51. Matsuguchi T, Musikacharoen T, Ogawa T, Yoshikai Y. 2000. Gene expressions of Toll-like receptor 2, but not Toll-like receptor 4, is induced by LPS and inflammatory cytokines in mouse macrophages. J Immunol 165:5767–5772. https://doi.org/10.4049/jimmunol.165.10.5767.
52. Bricker BJ, Ewalt DR, MacMillan AP, Foster G, Brew S. 2000. Molecular characterization of *Brucella* strains isolated from marine mammals. J Clin Microbiol 38:1258–1262.
53. Sheehan DC, Hrapchak BB. 1980. Theory and practice of histotechnology, 2nd ed. Battelle Press, Columbus, OH.
54. Crookham JN. 1991. Hazardous chemicals in the histopathology laboratory: regulations risks handling and disposal, 2nd ed. ANATECH, Battle Creek, MI.
55. Chiaraviglio L, Duong S, Brown DA, Birtles RJ, Kirby JE. 2010. An immunocompromised murine model of chronic *Bartonella* infection. Am J Pathol 176:2753–2763. https://doi.org/10.2353/ajpath.2010.090862.